First evidence of mesospheric hydroxyl response to electron precipitation from the radiation belts

Pekka T. Verronen,[1] Craig J. Rodger,[2] Mark A. Clilverd,[3] and Shuhui Wang[4]

P. T. Verronen, Earth Observation, Finnish Meteolorological Institute, P.O. Box 503, FI-00101 Helsinki, Finland. (pekka.verronen@fmi.fi)

C. J. Rodger, Department of Physics, University of Otago, P.O. Box 56, Dunedin, New Zealand. (crodger@physics.otago.ac.nz)

M. A. Clilverd, British Antractic Survey (NERC), High Cross, Madingley Road, Cambridge CB3 0ET, UK. (macl@bas.ac.uk)

S. Wang, Jet Propulsion Laboratory, 4800 Oak Grove Drive, Pasadena, CA 91109, USA. (shuhui.wang@jpl.nasa.gov)

[1]Earth Observation, Finnish Meteorological Institute, Helsinki, Finland

[2]Department of Physics, University of Otago, Dunedin, New Zealand

[3]British Antarctic Survey (NERC), Cambridge, UK

Abstract. Utilizing observations from the Medium Energy Proton and Electron Detector (MEPED) onboard the Polar Orbiting Environmental Satellite (POES) and the Microwave Limb Sounder (MLS) onboard the Aura satellite, we demonstrate that there is a strong link between 100 – 300 keV loss cone electron count rates observed in the outer radiation belt and night-time OH concentrations in the middle mesosphere at 71 – 78 km altitude. In theory, this can be expected because the ionization caused by energetic electron precipitation (EEP) leads to odd hydrogen (HO_x) production through ionic reactions. However, this is the first time that OH production due to EEP has been observed. We consider daily mean data from two months, March 2005 and April 2006, which were selected because of 1) relatively high count rates of radiation belt electrons observed 2) the absence of solar proton events that could mask the EEP effects. The results show that at 55 – 65° magnetic latitude (equivalent to McIlwain L shells 3.0 – 5.6) increases in electron count rates by two orders of magnitude are accompanied by increases in night-time OH concentration of 100%. There is a high correlation between MEPED and MLS data such that 56 – 87% of the OH variation can be explained by changes in EEP. Because the relation between MEPED count rate observations and

[4]Jet Propulsion Laboratory, California

Institute of Technology, Pasadena,

California, USA

the flux of electrons actually entering the atmosphere is not trivial, we discuss the possibility of using OH observations to obtain an estimate of EEP forcing that could be used in atmospheric modeling.

1. Introduction

Energetic particle precipitation occurring at high magnetic latitudes affects the neutral composition of the middle atmosphere. For example, ozone-destroying catalytic reactions take place after particle impact ionization and ion chemistry produce excess amounts of odd hydrogen (HO_x = H + OH + HO_2) and odd nitrogen (NO_x = N + NO + NO_2) species. In the upper stratosphere and mesosphere, substantial changes in ozone have been observed by satellites especially after large solar proton events [*Jackman et al.*, 2001; *Seppälä et al.*, 2004; *López-Puertas et al.*, 2005; *Verronen et al.*, 2006].

After ionization takes place, the NO_x production is mostly due to secondary electrons which efficiently dissociate N_2 molecules to yield atoms of nitrogen [*Porter et al.*, 1976; *Rusch et al.*, 1981]. Although the atoms in their ground state N(^{4}S) will react with NO causing NO_x loss, those in the excited state N(^{2}D) react with O_2 molecules and produce NO. Also ion chemistry, involving simple ions such as N^+ and NO^+, produces NO. Production of HO_x species is more complicated because it involves the formation of water cluster ions, such as $H^+(H_2O)_4$, which then recombine breaking H_2O molecules to yield OH and H [*Heaps*, 1978; *Solomon et al.*, 1981]. HO_x production takes place only at altitudes below $\approx$ 80 km where enough water vapor is available for efficient cluster ion formation.

The atmospheric effects caused by solar proton events (SPEs) are reasonably well known. This is because high-energy protons, although guided by the Earth's magnetic field into the high-latitude polar regions, propagate more or less directly from the Sun into Earth's atmosphere so that continuous proton flux observations made from Geostationary Orbit

can be used to calculate energy deposition and ionization rates at middle atmospheric altitudes. Also, detecting atmospheric effects of SPEs is relatively easy because they typically cover a large, continuous geographical area, i.e. the polar caps [*Jackman et al.*, 2001; *Rodger et al.*, 2006; *Verronen et al.*, 2007]. In contrast, energetic electrons are first captured and stored by Earth's magnetosphere, e.g. the radiation belts, from where they are eventually lost into the atmosphere especially during magnetic storms which can accelerate the electrons to high energies. The temporal variability, strength, and significance of energetic electron precipitation (EEP) reaching the mesosphere is poorly known because continuous flux measurements are particularly hard to make due to the relatively small size of the bounce loss cone at satellite altitudes (the loss cone is defined by the equatorial pitch angles of those electrons that will be lost to the atmosphere rather than be trapped by magnetic forces). Therefore, the calculation of atmospheric effects based on these data is not trivial. Electron fluxes could be estimated by radiation belt modeling, considering the balance of processes leading to input and loss of electrons in the belts, but large uncertainties are present in the current models [*Bourdarie et al.*, 2007].

Although there has been evidence that EEP is affecting polar NO_x and ozone in the mesosphere and upper stratosphere, the scarcity of the electron flux and atmospheric data has not allowed for strong conclusions on the significance of EEP in general [e.g. *Callis et al.*, 2001]. Recently, observations have shown that substantial amounts of NO_x have descended inside the polar vortex from mesosphere to stratosphere during most winters of the last decade [*Funke et al.*, 2005; *Seppälä et al.*, 2007; *Hauchecorne et al.*, 2007; *Randall et al.*, 2009]. Also, a high negative correlation has been found between the decadal winter-time variations of polar mid-stratospheric ozone and the flux of energetic electrons in the

radiation belts [*Sinnhuber et al.*, 2006]. Changes in stratospheric ozone could implicate changes in the general circulation and climate, but the connecting mechanisms are not yet understood. In order to adequately study these connections between atmospheric layers, it would be important to know the characteristics of EEP so that altitudes and locations of NO_x and HO_x production could be determined with confidence. This is not currently the case, and the relative importance of dynamical transport and in-situ production by particle precipitation to observed NO_x enhancements is not always clear.

In this paper, we investigate the connection between electron count rates and OH concentrations measured by MEPED/POES in the outer radiation belt and MLS/Aura in the mesosphere, respectively. We will show that there is a clear increase in OH during high-count-rate periods at magnetic latitudes 55 – 65°. We also discuss the possibility of using OH observations as an aid in the characterization of the energy, magnitude, and spatio-temporal extent of EEP.

2. Data

2.1. Electron count rates from MEPED/POES

The second generation of the Space Environment Monitor (SEM-2) onboard the NOAA Polar Orbiting Environment Satellites (POES) contains a Medium Energy Proton and Electron Detector (MEPED) that monitors the intensities of charged particle radiation at higher energies extending up to cosmic rays [*Evans and Greer*, 2004]. POES orbits the Earth in a high-inclination (polar), Sun-synchronous orbit at about 800 km altitude. MEPED has two electron telescopes and two proton telescopes. Both electron telescopes provide three channels of energetic electron data: >30 keV, >100 keV, and >300 keV. The channels are sampled simultaneously, so the number of data points is the same and data

from different channels are directly comparable in time and space. The difference between the pairs of telescopes is that they are pointed approximately perpendicular to each other. The so-called 0° electron detector views outward along the Earth-center-to-satellite vector. Whenever the satellite is poleward of a geomagnetic latitude of about 33°, this detector monitors electrons in the bounce loss cone that will enter the Earth's atmosphere below the satellite [*Rodger et al.*, 2010]. At lower latitudes, it measures electrons that are geomagnetically trapped. The response of the 90° detector is more complex; at high latitudes it tends to measure a combination of trapped and quasi-trapped electrons (i.e. electrons in the drift loss cone that are not lost to the atmosphere locally but are lost in regions where the magnetic field is weaker), and bounce loss cone electrons at low latitudes [*Rodger et al.*, 2010].

In this work we use data from the MEPED 0° electron telescope to monitor the electron precipitation in high-latitude regions. First, SEM-2 data of 16-second time resolution from NOAA-15, -16, and -17 were combined to produce 3-hour and further daily mean electron counts at L shells 3.0 – 5.6. These L values are equivalent to magnetic latitudes 55 – 65° (magnetic field lines cross the Earth's magnetic equator at a number of Earth-radii equal to their L value) and connect to the outer radiation belt. Then, energy channels >100 keV and >300 keV were used, and the count rate of the latter channel was subtracted from that of the former in order to get an estimate of the precipitating flux values for the 100 – 300 keV electrons. It should be noted that our approach, averaging each of the channels first and then subtracting, could introduce inconsistencies in the time/space sampling between the two energy channels. This is because on average (over time period 1998 – 2007) 3-hour data have significantly more corrupted data points in the >300keV channel

than in the >100keV channel due to proton contamination [*Rodger et al.*, 2010]. However, neither the 3-hour nor daily average data used in the present study are compromised by this issue. The atmospheric penetration depth of electrons depends upon their energy such that 40 keV, 100 keV, 300 keV, 1 MeV, and 3 MeV electrons deposit a major part of their energy (i.e. ionize atmospheric molecules) at approximately 90, 80, 70, 60 and 50 km, respectively, and have virtually no effect at the altitudes below [e.g. *Turunen et al.*, 2009, Fig. 3]. Therefore, the 100 – 300 keV electrons are affecting the atmosphere at $\approx$ 70 – 80 km. In principle, the electron flux units are $\mathrm{cm^{-2}\,s^{-1}\,sr^{-1}}$. However, the fraction of the loss cone viewed by the instrument will change with L shell, which means that it is not straight forward to establish a "true" precipitation flux. Nevertheless, the observations can be used to monitor changes in the levels of electron precipitation. It should be noted that electron fluxes from MEPED are not readily usable in atmospheric ionization rate calculations because of the issues above, and also due to degeneration of the instrument and data over time as well as significant levels of contamination by low-energy protons during storms times [*Rodger et al.*, 2010]. For this reason we will work in counts per second, rather than working with absolute flux values, while noting that the conversion from counts/s to "normal" electron flux units ($\mathrm{cm^{-2}\,s^{-1}\,sr^{-1}}$) simply involves multiplying the count rate by 100 [*Evans and Greer*, 2004].

SPEs, whenever they occur, dominate the ionization in the middle atmosphere. Therefore we made a search for times with high electron count rates, which indicate precipitation into the atmosphere, but with no SPEs. In Fig. 1, the POES daily mean count rate observations for years 2004 – 2007 are shown at $L = 3.0$ – 5.6 ($E > 300$ keV, 0° telescope), together with the occurrence of coronal mass ejections (CMEs) observed by the Advanced

Composition Explorer (ACE) satellite (red x marks). Although all CMEs do not lead to SPEs, we used them to exclude even the possibility of SPEs. At most times when the electron count is elevated, there is also a CME close by. Excluding these, the most pronounced electron count rates occur in March 2004, March 2005, and April 2006. Only the latter two are relevant for this study because the OH observations by MLS/Aura were started in August 2004. In addition to the CME screening, we also checked the 2.5 – 6.9 MeV and >5 MeV proton fluxes observed by POES and the GOES satellite, respectively (not shown). These fluxes are an indicator of possible forcing in the lower mesosphere because proton energies of 4 – 40 MeV are required in order to have energy deposition at $\approx$ 80 – 50 km, respectively [e.g. *Turunen et al.*, 2009]. Neither GOES nor POES observations show significantly enhanced proton fluxes in March 2005 or April 2006.

Before the analysis, we processed the MEPED/POES observations to exclude contamination by low-energy protons, following the simple procedure described by *Rodger et al.* [2010]. For the time periods studied here, the median reduction in electron count rates due to the proton screening is only $\sim$10% or less. This means that the low-energy proton contamination as well as the proton screening have, in the current study, a modest effect on the electron count rates.

2.2. OH concentrations from MLS/Aura

The Microwave Limb Sounder (MLS) instrument is onboard NASA's Aura satellite which was launched in July, 2004, into a Sun-synchronous near-polar orbit [*Waters et al.*, 2006]. MLS observations can be used to monitor a large number of trace gases of the middle atmosphere, which includes O_3, OH, HO_2, and H_2O. The instrument is able to measure during both day and night conditions, and the observations cover geographic

latitudes 82°S – 82°N on each orbit. MLS is the first satellite instrument providing continuous observations of OH and HO_2 in the mesosphere [*Pickett et al.*, 2006; *Pickett et al.*, 2008].

The HO_x family has a strong diurnal variation in the middle atmosphere because its production from H_2O depends upon solar radiation. In the stratosphere, water vapor is dissociated in reaction with $O(^1D)$ which is a product of O_3 photodissociation. In the mesosphere, direct photodissociation of H_2O by radiation at wavelengths shorter than 200 nm occurs. However, the corresponding HO_x production is diminished above 80 km where the H_2O concentration rapidly decreases with altitude. At night-time, when solar radiation is absent, the OH concentration typically decreases by an order of magnitude because the HO_x species are converted to H_2O and H_2 in reactions such as OH + HO_2 $\rightarrow$ H_2O + O_2. However, this behavior is reversed around 82 km where a sharp maximum layer of OH forms at night-time due to long-lived atomic hydrogen reacting with ozone [*Pickett et al.*, 2006].

OH observations made during solar proton events have shown that its concentration is sensitive to energetic particle precipitation [*Verronen et al.*, 2006; *Damiani et al.*, 2008]. Below $\approx$ 80 km, the chemical lifetime of the HO_x family is only on the order of hours. Therefore, transport processes play a minor role for the HO_x distribution on the short term. For these reasons, HO_x species are suitable for monitoring short-term variations of particle precipitation in the middle and lower mesosphere, and particularly for EEP.

In this paper, we utilize night-time observations of OH from MLS/Aura, data version 2.2x. The solar zenith angle at the point of observation was required to be larger than 100° and only local times between midnight and 6 a.m. were considered. These data

should typically show the lowest OH concentrations within a day (except at altitudes of the night-time OH layer), and make the detection of possible EEP-related enhancements easier. The estimated systematic error of the OH observations is typically within 8%, and validation has indicated a good agreement with balloon-borne and ground-based observations [*Pickett et al.*, 2008]. The vertical resolution of OH observations is $\sim$ 2.5 km. Corrupted data were screened out following the instructions of the MLS Data Quality and Description Document [*Livesey et al.*, 2007]. The geographic coordinates of the observations were converted to magnetic ones, so that the measurements can be sorted according to magnetic latitude. We made use of Corrected GeoMagnetic (CGM) coordinates based on the Definite/International Geomagnetic Reference Field (DGRF/IGRF) at 100 km altitude, determined using the GEOPACK software routines. MLS pressure levels and mixing ratios were converted to approximate altitudes and concentrations, respectively, using temperatures and total concentrations from the MSISE-90 model. As already discussed in Section 2.1, when comparing these OH data with particle count rate observations from MEPED it should be noted that electrons with energy between 100 and 300 keV will deposit their energy approximately at altitudes between 70 and 80 km [e.g. *Turunen et al.*, 2009, Fig. 3]. Because the formation of the OH night-time maximum at 82 km might complicate the detection of EEP effects we have, in most cases, excluded altitudes $\geq$80 km from our analysis. Therefore, we focus mainly on MLS hydroxyl data between 71 – 78 km (corresponding to pressure levels between 0.0464 – 0.0147 hPa).

In addition to OH, we also use MLS observations of water vapor (v2.2x) to support our discussions about OH variations. The H_2O data were sampled (SZA $> 100^\circ$, local times 0 – 6 a.m.), screened, and converted to concentrations and magnetic latitudes the same way

as we did it for the OH observations. In the mesosphere, the systematic errors of the H_2O observations are 6 – 34% and the vertical resolution is $\sim$ 12 – 16 km although the data are given in a grid of 3 – 5 km spacing [*Lambert et al.*, 2007]. Thus, the H_2O observations have a coarser retrieval pressure grid than what is used for OH. For this reason, in our analysis we use MLS water vapor data between 71 – 76 km (corresponding to pressure levels between 0.0464 – 0.0251 hPa), instead of using exactly the same altitude range as for OH.

3. Results

Taking into account the magnetic latitudes and altitudes that are likely to be affected by radiation belt electrons, we begin by plotting some of the electron count rate and OH data in the same figure. Fig. 2 shows daily average data from MEPED and MLS. In March 2005, mean electron count rates at $L = 3.0 - 5.6$ (magnetic latitudes 55 – 65°) vary by three orders of magnitude within this time period. The count rate is elevated especially from day 6 to 9 with count rates higher than 100 counts/s. The secondary peaks on days 14, 17, 26, and 31 show an order-of-magnitude lower count rates compared to the maximum on day 7. Similar temporal behavior is seen in OH observations at magnetic latitudes 55 – 65°N. The average concentration at 71 – 78 km (corresponding to the pressure levels of MLS observations at 0.0464, 0.0316, 0.0215, and 0.0146 hPa) ranges between 4.5×10^5 and 10.5×10^5 cm^{-3}, thus the variation is roughly within a factor of two. The largest OH concentrations, which significantly exceed the median of the daily values, are measured from day 6 to 9 and clearly coincide with the highest electron count rates. On the other days, the concentrations seem to follow the electron count rate changes in most cases, although the magnitude of variation is relatively low. At magnetic

latitudes 35 – 45°N, which are shown for comparison and are not expected to be affected by EEP, the OH concentration does not respond to the count rate increase of day 7. A similar investigation of April 2006 data shows the same behavior. A clear increase of OH concentration occurs at 55 – 65°N when electron count rate exceeds 100 counts/s on day 5, 14, and 15. At 35 – 45°N there is no response to count rate increase, as expected.

In order to better understand the latitude-longitude extent of the EEP effects, we next examine more closely the OH data from March 5 – 10, 2005. In Fig. 3, the observations at 71 – 78 km are averaged into geographic latitude-longitude grid and presented on a world map with approximate magnetic latitudes superimposed. In the polar regions, the Southern Hemisphere (SH) concentrations are generally higher than those of the Northern Hemisphere (NH). This is probably due to the middle atmosphere circulation, upwelling/downwelling in the summer/winter, bringing in air rich/poor in water vapor (source of HO_x) to these altitudes. Therefore, in this case we would expect to see more pronounced EEP effects in the north. In the SH, high OH concentrations follow magnetic rather than geographic latitudes, this is especially apparent at longitudes 30 – 180°. Highest values are seen at magnetic latitudes larger than 55°. In the NH, where the background OH concentration is lower, the higher OH concentration values are more clearly confined to the magnetic latitude band 55 – 65°. Enhancements are seen also at higher latitudes, at longitudes 0 – 150°, because EEP from the radiation belts is not strictly restricted to 55 – 65°. However, based on POES data (not shown), the high electron count rates are typically centered at L values 3 – 5.6 (magnetic latitudes 55 – 65°) making this the best region when studying EEP forcing. We have no clear explanation for the high OH values observed in the north coast of South America (0 – 20°N, 30 – 60°W,

geographic). They are possibly related to South Atlantic Magnetic Anomaly (SAMA), although it should be centered about 30° south of the high values. Note that these high values were observed in a descending orbit and MLS was looking forward (South). Therefore, the satellite was not in the SAMA region at that time. A preliminary investigation of the night-time OH data from the SAMA region indicates somewhat higher mixing ratios and larger variations than in other regions (not shown). However, more work would be needed in order to make more definite conclusions. Overall, the magnetic latitudes that we expect to be under the influence of EEP during this period show high concentrations of OH.

After pinpointing the EEP effects latitude-wise, we now study the EEP response at selected altitudes. Fig. 4 shows the daily mean OH concentrations in March 2005 at 55 – 65°N at 63 – 82 km versus daily mean MEPED 0° electron telescope count rate observations at L = 3.0 – 5.6. The pressure levels of MLS observations corresponding to the altitudes shown are given in the bottom right corner of the panels. Correlation coefficients r, random chance probability p (t-test), and line fit parameters a and b were calculated, the results are given in the panel titles. We consider the correlation to be high (i.e. not insignificant) when its p value is <5%. In the present study, this p limit corresponds to $r \approx 0.35$, thus larger r values indicate high correlation. In these calculations, we used square root of electron count rates based on the following simple estimation: assume that 1) the night-time HO_x production rate is proportional to the electron count rate R and 2) the loss is due to HO_x + HO_x reactions so that the loss rate is proportional to $[HO_x][HO_x]$. Then the concentration of odd hydrogen $[HO_x]$ should be proportional to $\sqrt{R}$. Therefore, the fit parameters a and b connect electron count rate and OH concen-

tration through [OH] = $(a \times \sqrt{R} + b) \times 10^5$ cm^{-3}. The correlation is high at 71 – 78 km, where $r = 0.71 - 0.73$ and indicates that about 52% ($= r^2$) of the OH variability can be explained by changes in EEP forcing. At 69 km and below, r is still high (i.e. larger than the 0.35 limit) but now only 14 – 35% of the OH variations can be explained by EEP. The correlation is low at 80 – 82 km because 1) the formation of the night-time narrow OH maximum masks EEP effects and 2) there is a lack of H_2O above 80 km so smaller amounts of water cluster ions are produced. The line fits at 71 – 78 km indicate that an increase in electron count rate by two orders of magnitude from 10 to 1000 counts/s more or less doubles the concentration of OH at most altitudes. Note that the fits show how zero-count-rate concentration, b, increases with altitude and is especially high at 80 – 82 km.

Looking next at a wider range of altitudes, Fig. 5 presents the altitude profiles of correlation coefficients for March 2005 and April 2006 at magnetic latitudes 55 – 65° (both N and S). In all cases, the correlation is positive and high, i.e. $r = 0.55$ – 0.90 at altitudes 71 – 78 km where the 100 – 300 keV electrons should have an impact. At altitudes 50 – 70 km, r is still high in most cases, i.e. ~ 0.5, which suggests that the EEP probably contained some amount of electrons with energies larger than 300 keV, more in April 2006 than in March 2005. On the other hand, the correlation is generally low below 50 km where > 2 MeV electrons would have an impact. It should be noted that in both cases, March 2005 and April 2006, the NH and SH show a similar behavior, giving more confidence in the results.

Based on the results above we are confident that OH concentrations at magnetic latitudes 55 – 65° and altitudes 71 – 78 km show a clear response to EEP as measured by

MEPED at $L = 3.0 - 5.6$. In Fig. 6 we again present comparisons with the MEPED electron count rate data, this time taking the mean of the OH data also over these altitudes. By averaging out over the altitude, the signal-to-noise ratio improves but, on the other hand, the natural variation may increase because OH concentration increases with increasing altitude (up to the 82-km night-time maximum). In any case, because the MEPED electron count rates are a total number for 100 – 300 keV energies it is logical to use averages of OH concentrations at the corresponding altitudes. In March 2005, the correlation between the data sets is as high as or higher than for most of the individual altitudes. For NH and SH, $r = 0.88$ and 0.75, respectively, thus EEP forcing can explain 77% and 56% of the OH variation. The slope of the fitted line a is 0.23 and 0.28 ($\times 10^5$) for the NH and SH, respectively. This means that OH changes corresponding to a change of count rate from 10 to 1000 counts/s are 6.5 and 7.9×10^5 cm^{-3}. In both hemispheres, the OH concentration is approximately doubled by such a count rate change. The results are similar for April 2006. The correlation is again high in both NH and SH ($r \geq 0.85$), so that EEP can explain 87% and 72% of the OH variations, respectively.

Comparing values of r and b in Fig. 6, it seems that in both March 2005 and April 2006 the correlation decreases as the background concentration of OH increases. This is understandable because in general there should be a threshold electron flux which must be exceeded if EEP is to produce enough OH to significantly enhance its concentration above the background. Therefore, the OH data corresponding to flux values lower than the threshold do not vary versus EEP. The higher the background concentration, the higher the flux must be to make a measurable impact. For example, in March 2005 the estimated OH background concentration at zero count rate, i.e. b, is about 50% higher in

the SH compared to the NH. So, in the SH the flux threshold is probably higher than in the NH and a larger portion of the OH observations are not significantly affected by EEP. Therefore, when including the low-count-rate data points, there should be less correlation in the SH, as there in fact is (see Fig. 6). To test this further, we excluded the data points with count rate lower than 10 counts/s and repeated the correlation calculations for March 2005. With this threshold applied, r increases in both NH and SH to 0.93 and 0.85, respectively, so that EEP now explains over 70% of the OH variation also in the SH. Raising the threshold even further leads to r values larger than 0.9 in both hemispheres. However, this improvement is at least partly due to the low number of data points remaining at high count rates.

Finally, we investigate the possible role of water vapor in the observed OH variations. A connection between OH and H_2O concentrations can obviously be expected because the former is photochemically produced from the latter. But could H_2O explain also the OH changes which we have attributed to EEP in this paper? The answer to the question is no, H_2O cannot explain these changes. However, in the following we show that it is nevertheless important to be aware of possible H_2O effects when looking for EEP signals in the OH data.

Fig. 7 shows daily mean MLS observations at magnetic latitudes 55 – 65°. The OH concentrations at 71 – 78 km are plotted against those of H_2O at 71 – 76 km (the altitude ranges we are using for OH and H_2O are not identical because the retrieval pressure grids of these two species are different, as pointed out in Section 2.2). The calculated r and p values are given inside each panel. In three of the four cases we find low correlation between OH and H_2O which gives further confidence in the role of EEP. However, in

March 2005, SH H_2O displays a wider range of concentrations compared to the other three cases, and there is a high, positive correlation between OH and H_2O ($r = 0.76$). Therefore, this case requires a closer examination.

In Fig. 8 we examine more carefully the variations of H_2O. The top panels show the monthly average global distribution at 71 – 76 km. In March 2005, there is $\sim 100\%$ more water vapor in the SH polar region compared to NH. This reflects the general meridional circulation in the mesosphere, from the summer pole to the winter pole, and explains the similar distribution of OH shown in Fig. 3, as discussed earlier. In contrast, in April 2006 the high-latitude H_2O amounts in the SH and NH are quite comparable, and clearly lower than the high values seen in SH in March 2005. Being later in the SH fall, April 2006 seems to reflect a transition phase which eventually leads to the reversal in the direction of the pole-to-pole circulation.

In the middle panels of Fig. 8, we present the daily 71 – 76 km mean H_2O values at magnetic latitudes 55 – 65°S. Clearly, the data for March 2005 and April 2006 show different behavior. In March 2005, H_2O gradually decreases by $\approx 25\%$, mostly during the second half of the month while in April 2006 the concentrations oscillate around the median of daily means. The gradual decrease, or trend, of H_2O in March 2005 affects OH, as we see in the panel c of Fig. 8. A decrease of $\approx 30\%$ occurs during the month, similarly to the decrease seen in H_2O. Therefore, it is evident that the trend explains the high correlation found between OH and H_2O in this case. In addition to the trend, the EEP effects can be seen in OH data especially when the electron count rates are at their peak around day 7.

In March 2005 there are two processes, i.e. EEP and the monthly trend of H_2O, that need to be considered in order to understand OH variations. In contrast, in the other three cases (NH data not shown) the relatively small H_2O changes leave EEP as the factor causing the largest OH variations. This difference, together with the differences in the general background concentration of H_2O/OH which we discussed earlier, is the reason why in March 2005 the SH hydroxyl data in Fig. 6 show more variability, less correlation with electron count rates, and larger uncertainty of the curve fit than in the other cases.

We also examined the role of temperature in OH variations at 71 – 78 km in the same manner as we did in the case of H_2O. A high negative correlation is found between OH and temperature, but again only in SH in March 2005 (not shown). However, the temperature increase even during March 2005, SH, is moderate, $\approx$ 8%. More importantly, there is a very high negative correlation ($<$ –0.95) between H_2O and temperature in March 2005 which is most likely of dynamical origin. The high/low values of temperature coinciding with the low/high values of H_2O in NH/SH are consistent with the expected effects of pole-to-pole circulation: adiabatic cooling/warming in the summer/winter pole due to upwelling/downwelling. Therefore, this indicates to us that the correlation found between OH and temperature is due to the dynamical connection between H_2O and temperature rather than the temperature changes having a significant effect on the chemical reaction rates. A more detailed analysis of the connection between temperature, H_2O, and OH would benefit from atmospheric modeling and is outside the scope of this paper.

4. Could EEP be characterized using OH observations?

As mentioned in the introduction, observations of EEP flux from satellites are not trivial and in most cases the data are not applicable to atmospheric modeling studies. In this section, we discuss the possibility of using satellite observations of hydroxyl as a proxy for EEP.

Monitoring the EEP forcing with OH observations is possible, in principle, because of its short chemical life-time. Unlike for many other species, e.g. NO_x, atmospheric transport plays no major role in short-term HO_x distribution of the lower mesosphere. However, HO_x is controlled on seasonal time scales by changes of water vapor. This can lead to significant differences in the background OH concentrations as was seen in March 2005 (see Fig. 3).

In Section 3 we showed that detection of EEP-related changes in night-time OH is practical at altitudes below 80 km. This means that only electrons with energies greater than 100 keV can be considered and lower-energy electrons, such as those creating aurora at ~ 100 km, are excluded. However, the effects of very high-energy electrons ($E > 1$ MeV, i.e. highly relativistic electrons) could possibly be studied because MLS observations extend down to ≈ 30 km.

The results show that within the electron count rate range observed here, OH concentration changes by about 100% (Fig. 6). The major part of the OH changes occur only at high count rate values, so that only effects of relatively strong EEP can be detected. Based on the line fits and the estimated standard deviations, count rates lower than 10 – 30 counts/s (as observed by MEPED) are not distinguishable using OH data. As

discussed earlier, the background level of OH determines this detection threshold which would therefore vary, e.g., with season of year.

Since the MEPED data do not represent real precipitation flux in absolute numbers, an atmospheric model would be needed to make a connection between precipitation fluxes and OH concentrations. EEP input would need to be varied so that flux threshold values in different conditions can be determined and the energy-flux spectrum of electrons can be solved. Clearly, larger data sets should be used in order to provide electron spectra for longer periods of time. This would aid the assessment of EEP importance in general in the context of atmospheric chemistry.

5. Conclusions

We have shown that there is a strong link between mesospheric night-time OH concentration at 71 – 78 km altitude and 100 – 300 keV count rate of electrons precipitating into the atmosphere from the radiation belts. This is the first evidence of a direct HO_x response to energetic electron precipitation, and a strong indication that EEP can drive significant *in-situ* changes in neutral atmospheric chemistry. The well-known mechanism causing the HO_x increase is ionization of atmospheric molecules by energetic particles which leads to ion chemical production of odd hydrogen from water vapor.

In this study we used OH data from MLS/Aura and electron count rates from MEPED/POES, concentrating on magnetic latitudes 55 – 65°. In the cases studied, i.e. March 2005 and April 2006, the OH concentrations were enhanced when high electron count rates were observed. The correlation between the count rate and OH data was found to be positive and high such that 56 – 87% of the OH variation can be explained by

EEP. This percentage depends on the background concentration of OH which determines the threshold flux of electrons.

Satellite observations of EEP are typically not directly usable in atmospheric modeling. For example, the connection between the real precipitation flux and MEPED observations is not trivial. In future, it might be possible, and very useful, to determine EEP fluxes from OH observations, if an atmospheric model is first used to study the sensitivity of OH to EEP in different conditions.

Acknowledgments. PTV would like to thank Dr. Marko Laine for valuable discussions. The work of PTV was supported by the Academy of Finland through the projects #136225/SPOC (Significance of Energetic Electron Precipitation to Odd Hydrogen, Ozone, and Climate) and #123275/THERMES (Thermosphere and Mesosphere Affecting the Stratosphere). Research at the Jet Propulsion Laboratory, California Institute of Technology, is performed under contract with the National Aeronautics and Space Administration. POES data were provided by NOAA National Geophysical Data Center. MLS/Aura data were provided by the NASA Goddard Earth Sciences Data and Information Service Center (GES DISC).

References

Bourdarie, S., V. Maget, R. Friedel, D. Boscher, A. Sicard, and D. Lazaro (2007), Complementarity of measurements and models in reproducing Earth's radiation belt dynamics, in *Space Weather*, *Astrophysics and Space Science Library*, vol. 322, edited by J. Lilensten, pp. 219–229, Springer, Dordrecht, The Netherlands.

Callis, L. B., M. Natarajan, and J. D. Lambeth (2001), Solar-atmospheric coupling by electrons (SOLACE): 3. Comparisons of simulations and observations, 1979-1997, issues and implications, *J. Geophys. Res.*, *106*, 7523–7540.

Damiani, A., M. Storini, M. Laurenza, and C. Rafanelli (2008), Solar particle effects on minor components of the Polar atmosphere, *Ann. Geophys.*, *26*, 361–370.

Evans, D. S., and M. S. Greer (2004), Polar orbiting environmental satellite space environment monitor – 2 instrument descriptions and archive data documentation, NOAA Technical Memorandum version 1.4, Space Environment Laboratory, Colorado.

Funke, B., M. López-Puertas, S. Gil-Lopez, T. von Clarmann, G. P. Stiller, H. Fischer, and Kellmann (2005), Downward transport of upper atmospheric NOx into the polar stratosphere and lower mesosphere during the Antarctic 2003 and Arctic 2002/2003 winters, *J. Geophys. Res.*, *110*(D24), D24,308, doi:10.1029/2005JD006463.

Hauchecorne, A., J.-L. Bertaux, F. Dalaudier, J. M. Russell, M. G. Mlynczak, E. Kyrölä, and D. Fussen (2007), Large increase of NO_2 in the north polar mesosphere in January-February 2004: Evidence of a dynamical origin from GOMOS/ENVISAT and SABER/TIMED data, *Geophys. Res. Lett.*, *34*, 3810, doi:10.1029/2006GL027628.

Heaps, M. G. (1978), The effect of a solar proton event on the minor neutral constituents of the summer polar mesosphere, *Rep. ASL-TR0012*, U.S. Army Atmos. Sci. Lab., White Sands Missile Range, N. M.

Jackman, C. H., R. D. McPeters, G. J. Labow, E. L. Fleming, C. J. Praderas, and J. M. Russel (2001), Northern hemisphere atmospheric effects due to the July 2000 solar proton events, *Geophys. Res. Lett.*, *28*, 2883–2886.

Lambert, A., et al. (2007), Validation of the Aura Microwave Limb Sounder middle atmosphere water vapor and nitrous oxide measurements, *J. Geophys. Res.*, *112*, D24S32, doi:10.1029/2007JD008724.

Livesey, N. J., et al. (2007), EOS MLS Version 2.2 Level 2 data quality and description document, JPL D-33509, Jet Propulsion Laboratory, Version 2.2x-1.0a, May 22.

López-Puertas, M., B. Funke, S. Gil-López, T. von Clarmann, G. P. Stiller, M. Höpfner, S. Kellmann, H. Fischer, and C. H. Jackman (2005), Observation of NO_x enhancement and ozone depletion in the northern and southern hemispheres after the October-November 2003 solar proton events, *J. Geophys. Res.*, *110*, A09S43, doi: 10.1029/2005JA011050.

Pickett, H. M., W. G. Read, K. K. Lee, and Y. L. Yung (2006), Observation of night OH in the mesosphere, *Geophys. Res. Lett.*, *33*, L19,808, doi:10.1029/2006GL026910.

Pickett, H. M., et al. (2008), Validation of Aura Microwave Limb Sounder OH and HO_2 measurements, *J. Geophys. Res.*, *113*, D16S30, doi:10.1029/2007JD008775.

Porter, H. S., C. H. Jackman, and A. E. S. Green (1976), Efficiencies for production of atomic nitrogen and oxygen by relativistic proton impact in air, *J. Chem. Phys.*, *65*, 154–167.

Randall, C. E., V. L. Harvey, D. E. Siskind, J. France, P. F. Bernath, C. D. Boone, and K. A. Walker (2009), NO_x descent in the Arctic middle atmosphere in early 2009, *Geophys. Res. Lett.*, *36*, L18,811, doi:10.1029/2009GL039706.

Rodger, C. J., M. A. Clilverd, P. T. Verronen, T. Ulich, M. J. Jarvis, and E. Turunen (2006), Dynamic geomagnetic rigidity cutoff variations during a solar proton event, *J. Geophys. Res.*, *111*, A04,222, doi:10.1029/2005JA011395.

Rodger, C. J., M. A. Clilverd, J. C. Green, and M. M. Lam (2010), Use of POES SEM-2 observations to examine radiation belt dynamics and energetic electron precipitation into the atmosphere, *J. Geophys. Res.*, *115*, A04,202, doi:10.1029/2008JA014023.

Rodger, C. J., B. R. Carson, S. A. Cummer, R. J. Gamble, M. A. Clilverd, J.-A. Sauvaud, M. Parrot, J. C. Green, and J.-J. Berthelier (2010), Contrasting the efficiency of radiation belt losses caused by ducted and non-ducted whistler mode waves from ground-based transmitters, *J. Geophys. Res.*, doi:10.1029/2010JA015880, in press.

Rusch, D. W., J.-C. Gérard, S. Solomon, P. J. Crutzen, and G. C. Reid (1981), The effect of particle precipitation events on the neutral and ion chemistry of the middle atmosphere – I. Odd nitrogen, *Planet. Space Sci.*, *29*, 767–774.

Seppälä, A., P. T. Verronen, E. Kyrölä, S. Hassinen, L. Backman, A. Hauchecorne, J. L. Bertaux, and D. Fussen (2004), Solar Proton Events of October-November 2003: Ozone depletion in the Northern hemisphere polar winter as seen by GOMOS/Envisat, *Geophys. Res. Lett.*, *31*(19), L19,107, doi:10.1029/2004GL021042.

Seppälä, A., P. T. Verronen, M. A. Clilverd, C. E. Randall, J. Tamminen, V. F. Sofieva, L. Backman, and E. Kyrölä (2007), Arctic and Antarctic polar winter NO_x and energetic particle precipitation in 2002–2006, *Geophys. Res. Lett.*, *34*, L12,810, doi:10.1029/2007GL029733.

Sinnhuber, B.-M., P. von der Gathen, M. Sinnhuber, M. Rex, G. König-Langlo, and S. J. Oltmans (2006), Large decadal scale changes of polar ozone suggest solar influence, *Atmos. Chem. Phys.*, *6*, 1835–1841.

Solomon, S., D. W. Rusch, J.-C. Gérard, G. C. Reid, and P. J. Crutzen (1981), The effect of particle precipitation events on the neutral and ion chemistry of the middle

atmosphere: II. Odd hydrogen, *Planet. Space Sci.*, *8*, 885–893.

Turunen, E., P. T. Verronen, A. Seppälä, C. J. Rodger, M. A. Clilverd, J. Tamminen, C.-F. Enell, and T. Ulich (2009), Impact of different precipitation energies on NO_x generation during geomagnetic storms, *J. Atmos. Terr. Phys.*, *71*, 1176–1189, doi: 10.1016/j.jastp.2008.07.005.

Verronen, P. T., A. Seppälä, E. Kyrölä, J. Tamminen, H. M. Pickett, and E. Turunen (2006), Production of odd hydrogen in the mesosphere during the January 2005 solar proton event, *Geophys. Res. Lett.*, *33*, L24,811, doi:10.1029/2006GL028115.

Verronen, P. T., C. J. Rodger, M. A. Clilverd, H. M. Pickett, and E. Turunen (2007), Latitudinal extent of the January 2005 solar proton event in the Northern Hemisphere from satellite observations of hydroxyl, *Ann. Geophys.*, *25*, 2203–2215.

Waters, J. W., et al. (2006), The Earth Observing System Microwave Limb Sounder (EOS MLS) on the Aura Satellite, *IEEE Trans. Geosci. Remote Sens.*, *44*, 1075–1092, doi:10.1109/TGRS.2006.873771.

Figure 1. Daily mean electron count rates observed by MEPED between 2004 and 2007 (black line). The times of coronal mass ejections are indicated with red x marks.

Figure 2. (a) and (d) Electron count rates (E = 100 – 300 keV). X = 3-hour mean values, solid line = daily mean. N = number of data points/day, standard error of the mean varies between 5% and 95%. (b) and (e) Mean OH concentrations at 71 – 78 km altitude and magnetic latitudes 55 – 65°N. Solid line = daily mean, dashed line = median of the daily mean values. N = median of data points/day, standard error of the mean is 7 – 10%. (c) and (f) Same as b and e but at magnetic latitudes 35 – 45°N.

Figure 3. Mean night-time OH concentration at 71 – 78 km on March 5 – 10, 2005. Approximate magnetic latitudes are indicated by superimposed white lines. Each latitude-longitude average is made of 144 – 220 data points (4 altitudes times 36 – 55 profiles), standard error of the mean is 7 – 15%. White areas indicate locations where the number of data profiles was less than 10, i.e. significantly lower than for the other locations.

Figure 4. OH concentrations versus electron count rates in March 2005 at magnetic latitudes 55 – 65°N. Dots = daily mean, black horizontal and vertical lines = standard error of the mean. The solid and dashed curves = fit to the data points and estimated standard deviation, respectively. In panel titles, r = correlation coefficient, p = probability of getting such correlation by random chance when true correlation is zero (t-test), a and b are line fit coefficients, i.e. $[\mathrm{OH}] = (a \times \sqrt{\mathrm{CountRate}} + b) \times 10^5$ cm^{-3}.

Figure 5. Correlation coefficients for the daily mean values of electron count rate and hydroxyl concentration at 30 – 90 km. The circled points indicate the correlations with a possibility of getting the coefficient by random chance less than 5% (t-test).

Figure 6. OH concentration at 71 – 78 km versus electron count rate. Dots = daily mean, black horizontal and vertical lines = standard error of the mean. The solid and dashed curves = fit to the data points and estimated standard deviation, respectively. In panels, top left corner, r = correlation coefficient, p = probability of getting such correlation by random chance when true correlation is zero (t-test), a and b are line fit coefficients, i.e. $[\mathrm{OH}] = (a \times \sqrt{\mathrm{CountRate}} + b) \times 10^5$ cm^{-3}.

Figure 7. OH concentration at 71 – 78 km versus H_2O concentration at 71 – 76 km (MLS observations). Dots = daily mean, black horizontal and vertical lines = standard error of the mean. Inside panels: r = correlation coefficient and p = probability of getting such correlation by random chance when true correlation is zero (t-test).

Figure 8. (a) and (d) Monthly mean H_2O concentrations at 71 – 76 km in March 2005 and April 2006, respectively. Each latitude-longitude average is made of 58 – 542 data points (2 altitudes times 29 – 271 profiles), standard error of the mean is 2 – 7%. White areas indicate locations with no night-time data (night-time = SZA $>$ 100°, local times 0 – 6 a.m.). (b) and (e) H_2O concentration at magnetic latitudes 55 – 65°S. Solid line = daily mean at 71 – 76 km, dashed line = median of the daily mean values. N = median of data points/day, standard error of the mean is 3 – 4%. (c) and (f) Same as b and e but for OH at 71 – 78 km. Standard error of the mean is 5 – 9%.

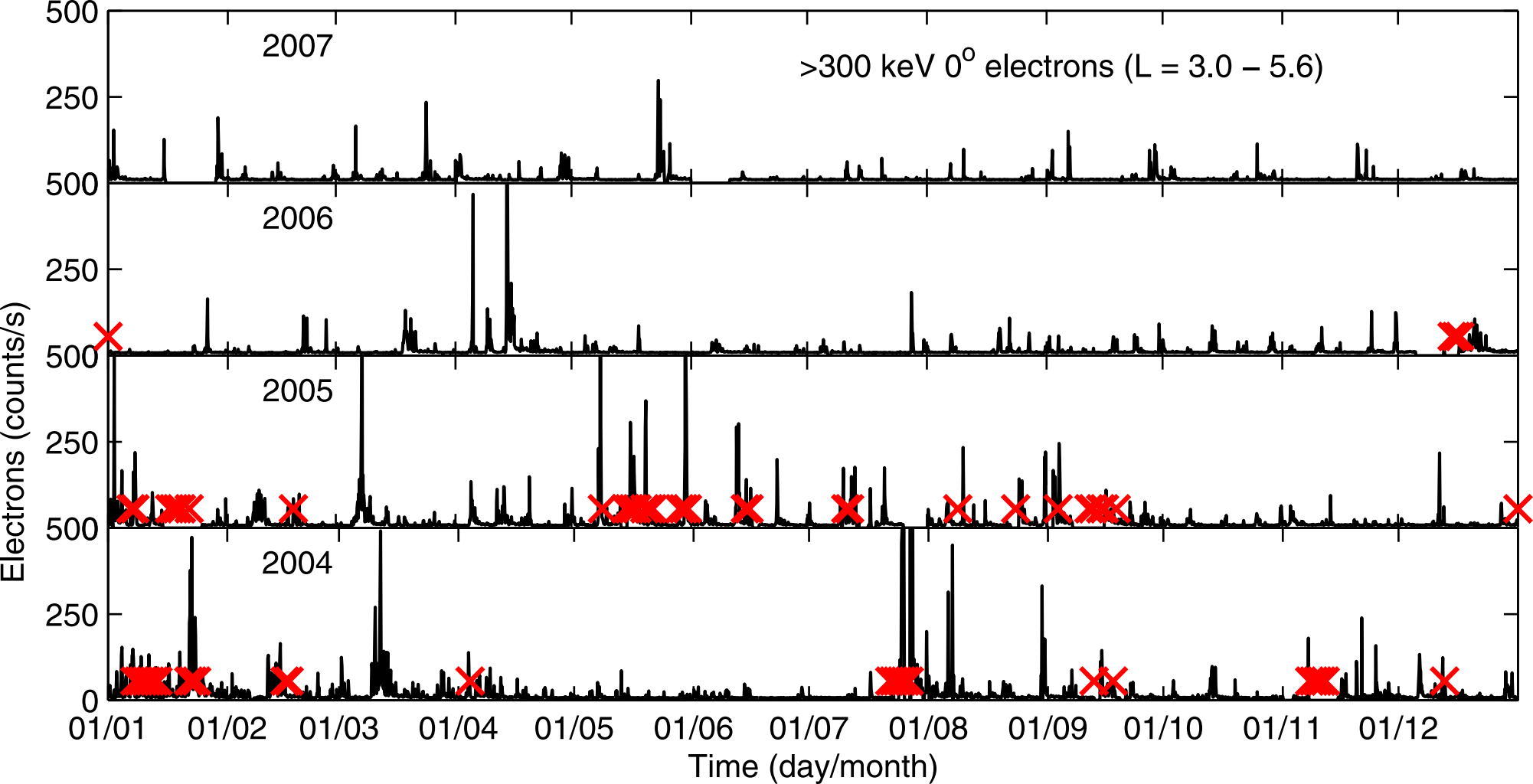
2007
>300 keV 0° electrons (L = 3.0 – 5.6)
2006
2005
2004
500
250
0
Electrons (counts/s)
01/01
01/02
01/03
01/04
01/05
01/06
01/07
01/08
01/09
01/10
01/11
01/12
Time (day/month)

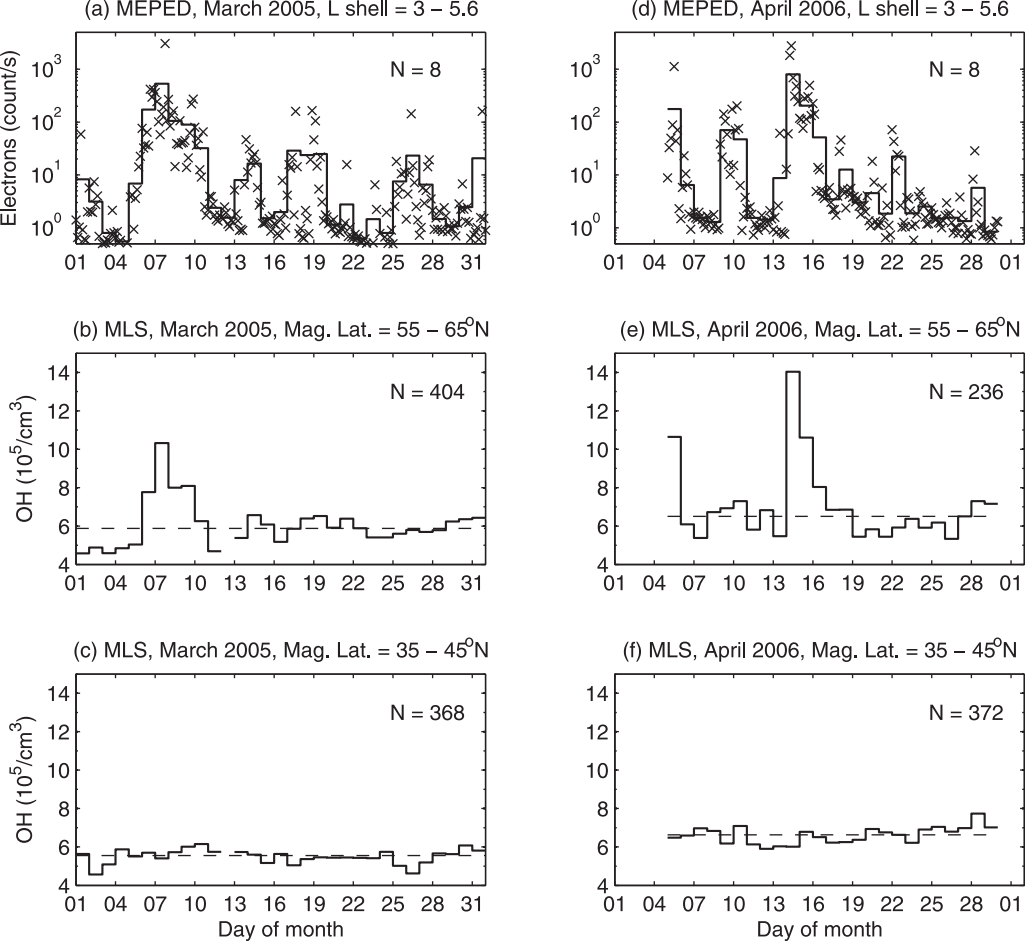
(a) MEPED, March 2005, L shell = 3 – 5.6
Electrons (count/s)
N = 8
(d) MEPED, April 2006, L shell = 3 – 5.6
N = 8
(b) MLS, March 2005, Mag. Lat. = 55 – 65°N
OH (10^5/cm^3)
N = 404
(e) MLS, April 2006, Mag. Lat. = 55 – 65°N
N = 236
(c) MLS, March 2005, Mag. Lat. = 35 – 45°N
N = 368
(f) MLS, April 2006, Mag. Lat. = 35 – 45°N
N = 372
Day of month
Day of month

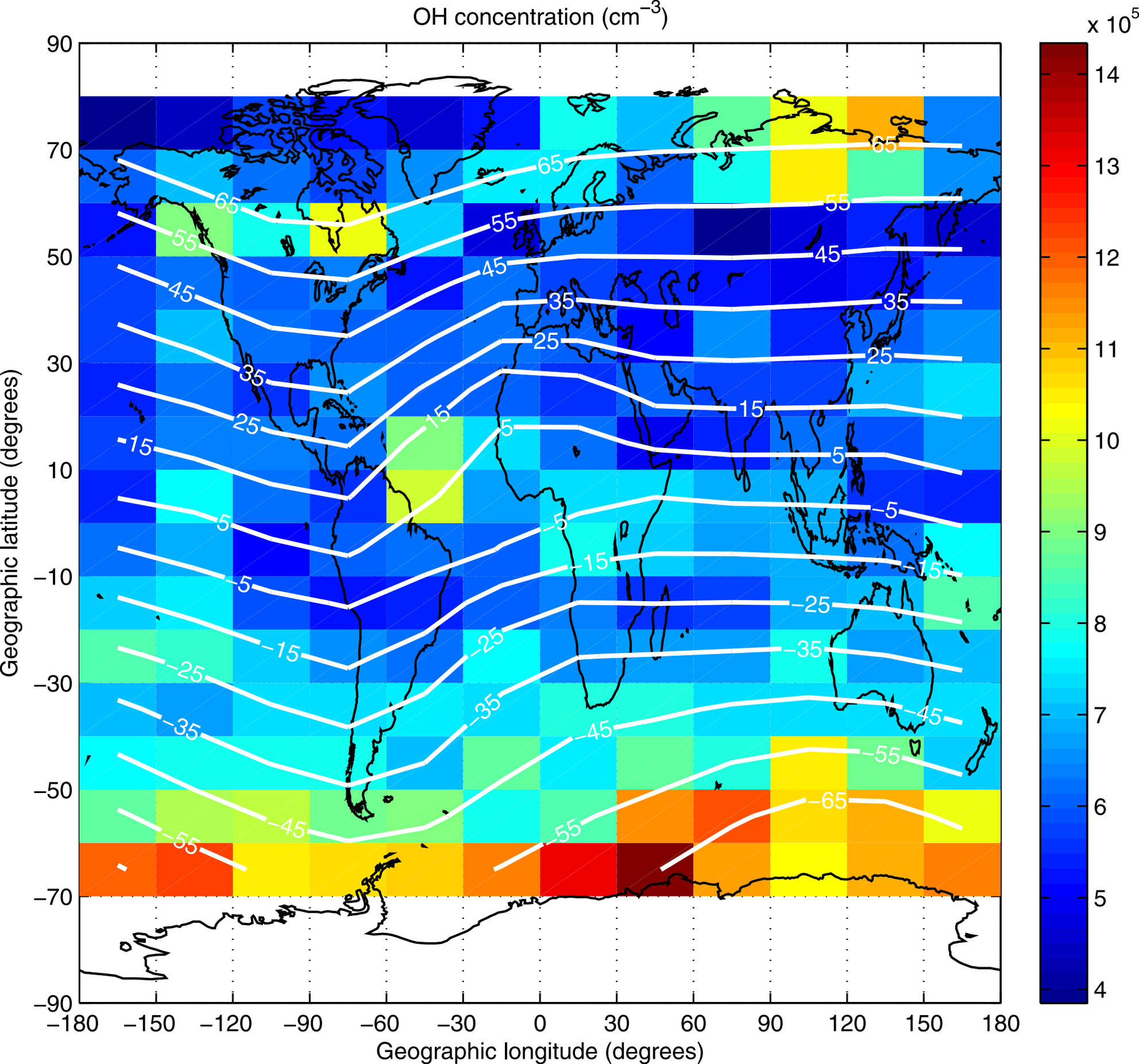
OH concentration (cm^{-3})
x 10^5
14
13
12
11
10
9
8
7
6
5
4
90
70
50
30
10
−10
−30
−50
−70
−90
Geographic latitude (degrees)
−180
−150
−120
−90
−60
−30
0
30
60
90
120
150
180
Geographic longitude (degrees)
65
55
45
35
25
15
5
−5
−15
−25
−35
−45
−55
−65

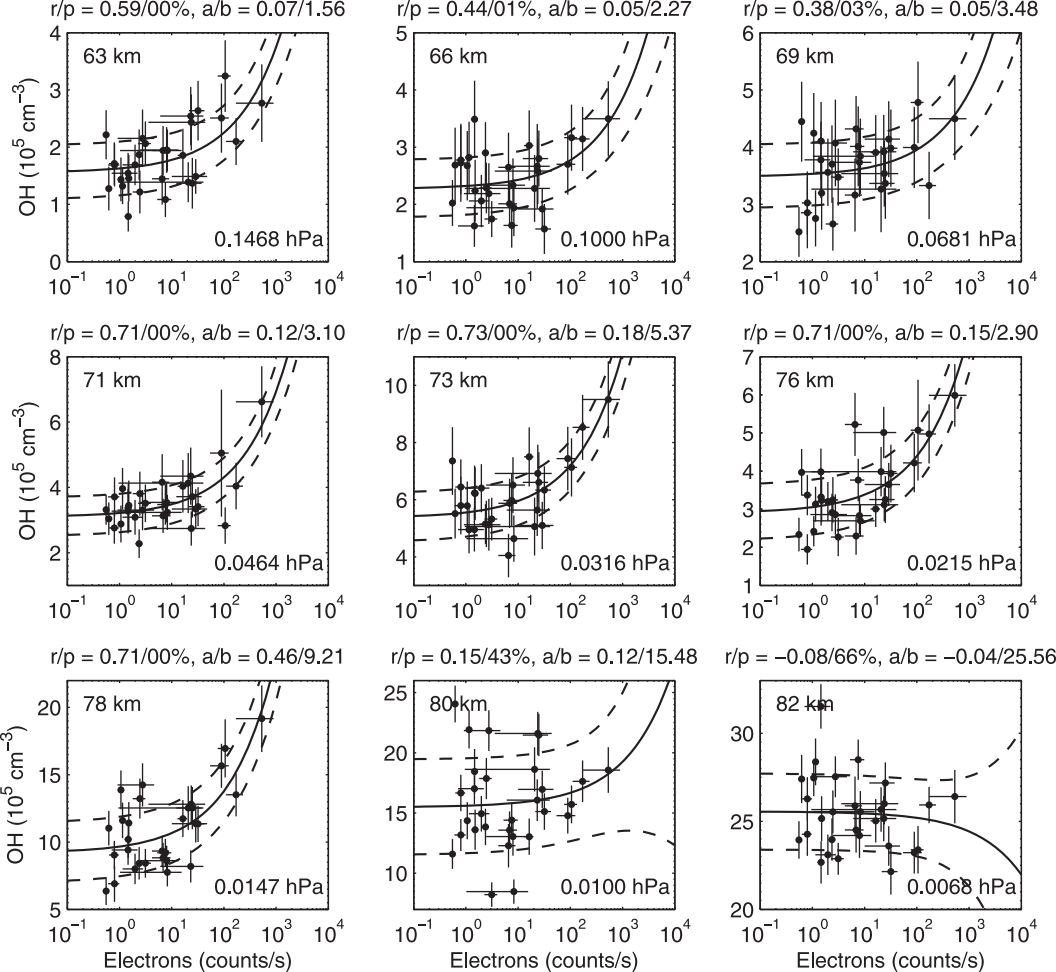
r/p = 0.59/00%, a/b = 0.07/1.56
63 km
0.1468 hPa
r/p = 0.44/01%, a/b = 0.05/2.27
66 km
0.1000 hPa
r/p = 0.38/03%, a/b = 0.05/3.48
69 km
0.0681 hPa
r/p = 0.71/00%, a/b = 0.12/3.10
71 km
0.0464 hPa
r/p = 0.73/00%, a/b = 0.18/5.37
73 km
0.0316 hPa
r/p = 0.71/00%, a/b = 0.15/2.90
76 km
0.0215 hPa
r/p = 0.71/00%, a/b = 0.46/9.21
78 km
0.0147 hPa
r/p = 0.15/43%, a/b = 0.12/15.48
80 km
0.0100 hPa
r/p = −0.08/66%, a/b = −0.04/25.56
82 km
0.0068 hPa
OH (10^5 cm^−3)
Electrons (counts/s)

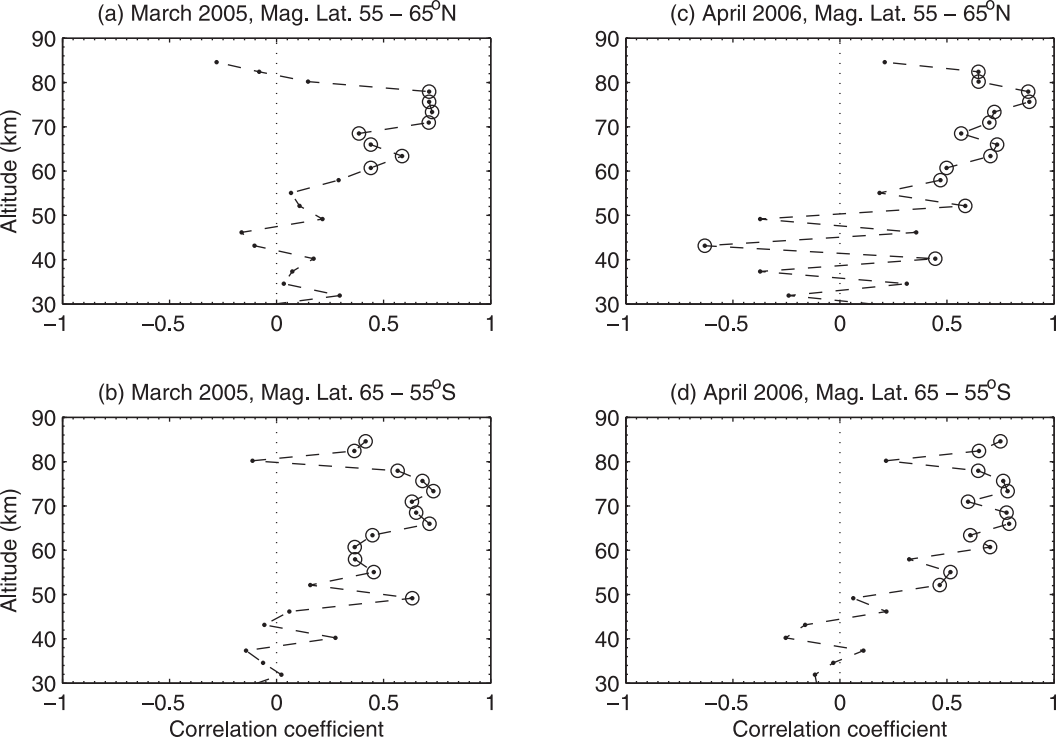
(a) March 2005, Mag. Lat. 55 – 65°N
(c) April 2006, Mag. Lat. 55 – 65°N
(b) March 2005, Mag. Lat. 65 – 55°S
(d) April 2006, Mag. Lat. 65 – 55°S
Altitude (km)
Correlation coefficient
90
80
70
60
50
40
30
−1
−0.5
0
0.5
1

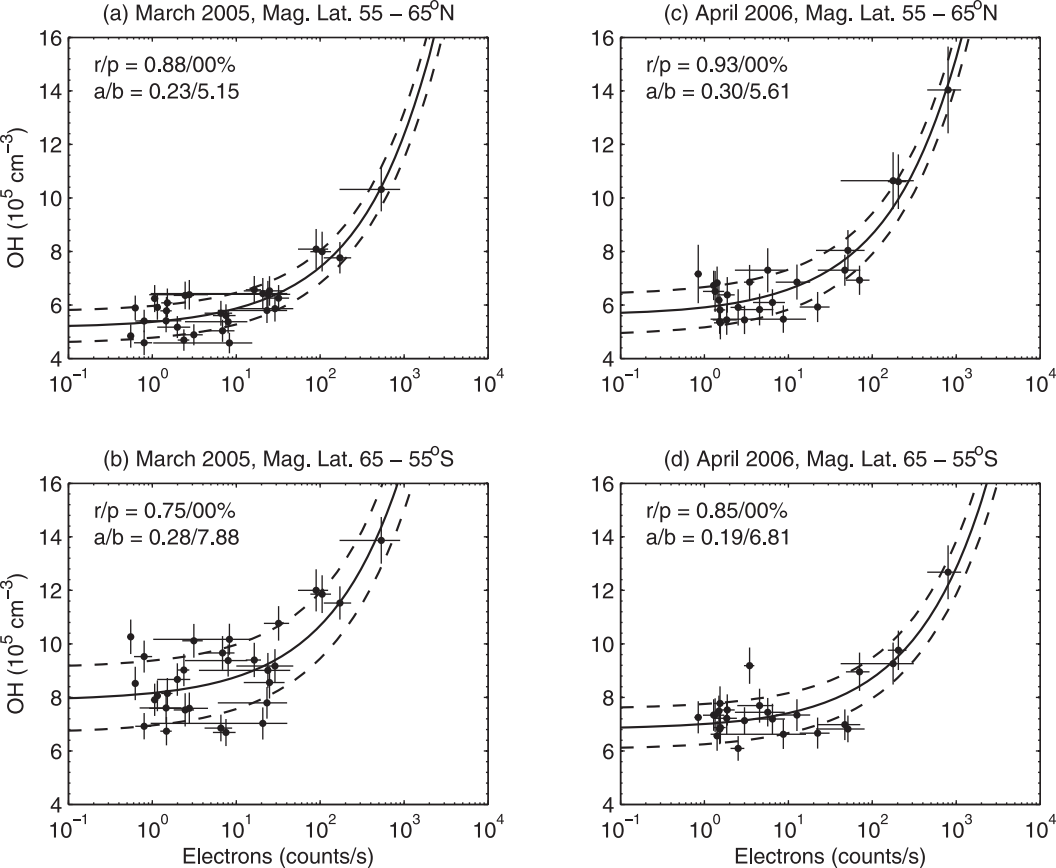
(a) March 2005, Mag. Lat. 55 – 65°N
r/p = 0.88/00%
a/b = 0.23/5.15
(c) April 2006, Mag. Lat. 55 – 65°N
r/p = 0.93/00%
a/b = 0.30/5.61
(b) March 2005, Mag. Lat. 65 – 55°S
r/p = 0.75/00%
a/b = 0.28/7.88
(d) April 2006, Mag. Lat. 65 – 55°S
r/p = 0.85/00%
a/b = 0.19/6.81
OH (10^5 cm^-3)
Electrons (counts/s)

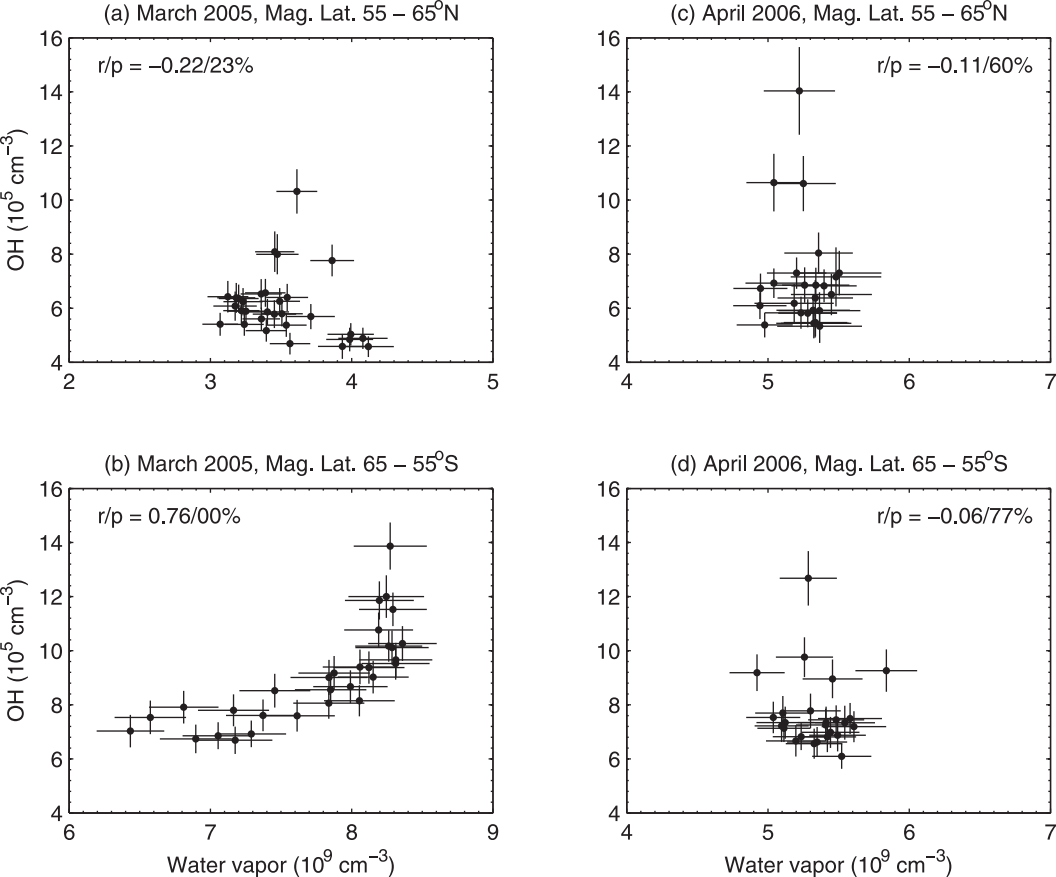
(a) March 2005, Mag. Lat. 55 – 65°N
r/p = –0.22/23%
(c) April 2006, Mag. Lat. 55 – 65°N
r/p = –0.11/60%
(b) March 2005, Mag. Lat. 65 – 55°S
r/p = 0.76/00%
(d) April 2006, Mag. Lat. 65 – 55°S
r/p = –0.06/77%
OH (10^5 cm^-3)
Water vapor (10^9 cm^-3)

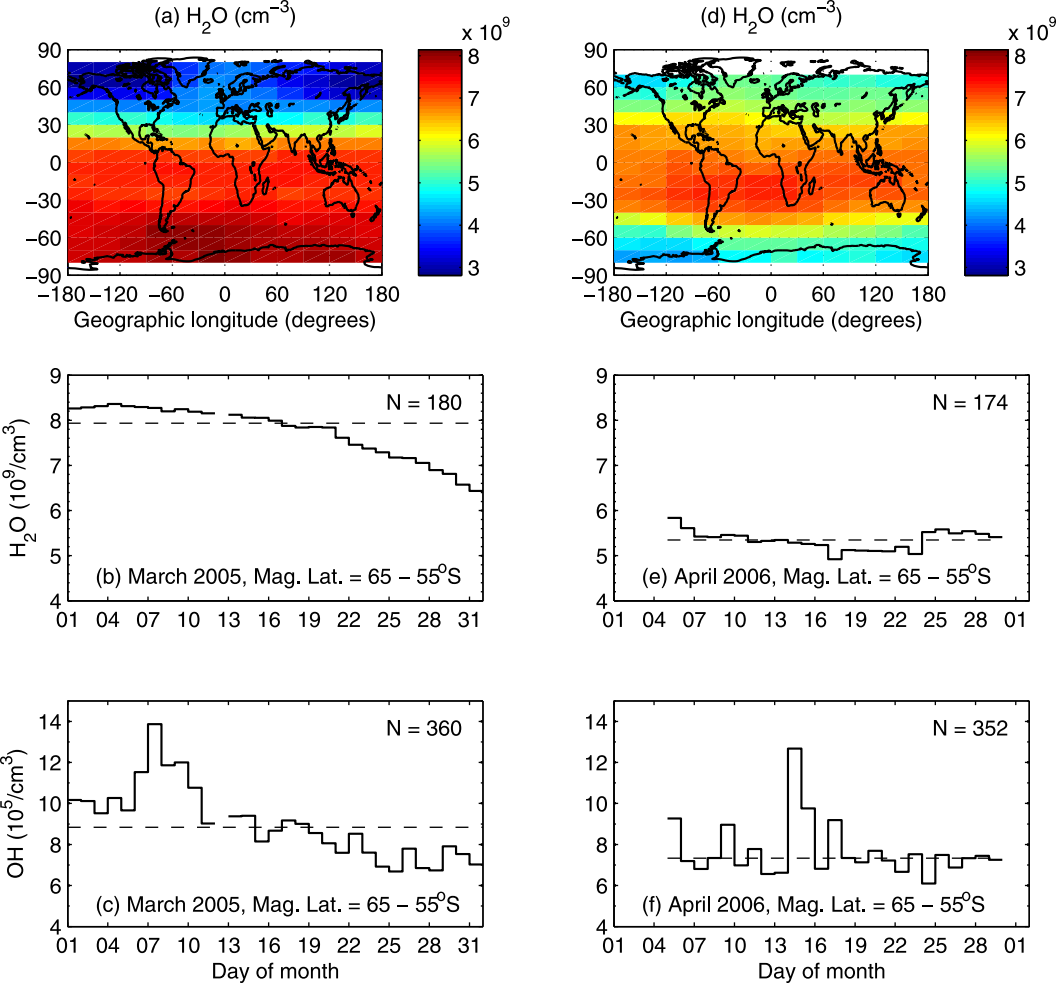
(a) H2O (cm−3)
x 10^9
8
7
6
5
4
3
90
60
30
0
−30
−60
−90
−180 −120 −60 0 60 120 180
Geographic longitude (degrees)
(d) H2O (cm−3)
x 10^9
Geographic longitude (degrees)
H2O (10^9/cm^3)
N = 180
(b) March 2005, Mag. Lat. = 65 – 55°S
N = 174
(e) April 2006, Mag. Lat. = 65 – 55°S
OH (10^5/cm^3)
N = 360
(c) March 2005, Mag. Lat. = 65 – 55°S
N = 352
(f) April 2006, Mag. Lat. = 65 – 55°S
01 04 07 10 13 16 19 22 25 28 31
Day of month